OPEN ACCESS

sensors

Article

Modelling of Amperometric Biosensor Used for Synergistic Substrates Determination

Dainius Simelevicius [1,*], Romas Baronas [1] and Juozas Kulys [2]

[1] Faculty of Mathematics and Informatics, Vilnius University, Naugarduko 24, LT-03225 Vilnius, Lithuania; E-Mail: romas.baronas@mif.vu.lt

[2] Institute of Biochemistry, Vilnius University, Mokslininku 12, LT-08662 Vilnius, Lithuania; E-Mail: juozas.kulys@bchi.vu.lt

[*] Author to whom correspondence should be addressed; E-Mail: dainius.simelevicius@mif.vu.lt; Tel.: +370-5-219-30-64; Fax: +370-5-215-15-85.

Abstract: In this paper the operation of an amperometric biosensor producing a chemically amplified signal is modelled numerically. The chemical amplification is achieved by using synergistic substrates. The model is based on non-stationary reaction-diffusion equations. The model involves three layers (compartments): a layer of enzyme solution entrapped on the electrode surface, a dialysis membrane covering the enzyme layer and an outer diffusion layer which is modelled by the Nernst approach. The equation system is solved numerically by using the finite difference technique. The biosensor response and sensitivity are investigated by altering the model parameters influencing the enzyme kinetics as well as the mass transport by diffusion. The biosensor action was analyzed with a special emphasis to the effect of the chemical amplification. The simulation results qualitatively explain and confirm the experimentally observed effect of the synergistic substrates conversion on the biosensor response.

Keywords: modelling; simulation; reaction-diffusion; biosensor; synergistic substrates

1. Introduction

A biosensor is an electronic measuring device designed for measurement of the concentration of some specific substance (analyte) in a solution. The device specificity for a particular substance is achieved by some biological material, usually an enzyme [1–3]. An amperometric biosensor assesses the concentration of the analyte through the measurement of the current on a working electrode [4,5]. Biosensors are widely used in various applications that require fast quantitative analysis [6–10].

Oxidases are the kind of enzymes commonly used in biosensors. In the case of oxidases, molecules of an enzyme are reduced to their intermediate state and then oxidised by electron acceptors [5,11]. The reduction process as a rule is a specific reaction, while the oxidation of the reduced enzyme by electron acceptors is less specific. Many electron acceptors can be employed in this process [12].

The kinetic analysis of the reaction of a mixture of low and high reactive electron acceptors shows that the reduction of a low reactive electron acceptor may substantially increase if the rate of the cross reaction between these substances is high enough. This phenomenon is employed in biosensors for a high sensitivity determination of synergistic substrates [13–15].

The understanding of the kinetic peculiarities of the biosensors is of crucial importance for their design and optimization. To improve the productivity as well as the efficiency of the biosensor design, a model of the biosensor should be built [16,17]. Starting from the seventies various mathematical models have been widely used as important tools to study and optimize analytical characteristics of actual biosensors [18–22]. A comprehensive reviews on the modelling of the amperometric biosensors have been presented in [23,24]. Biosensors based on synergistic substrates were modelled at steady-state conditions a few years ago [25,26]. Very recently, a laccase-based biosensor utilizing simultaneous substrates conversion was numerically modelled at steady-state as well as transient conditions [27].

The goal of this investigation was to develop a computational model for an effective simulation of amperometric biosensors utilizing the synergistic substrates conversion as well as to investigate the influence of the physical and kinetic parameters on the biosensor response. The developed model is based on non-stationary reaction-diffusion equations [28,29]. The mathematical model comprises three compartments, a layer of enzyme solution entrapped on the electrode surface, a dialysis membrane covering the enzyme layer and an outer diffusion layer. By changing input parameters the output results were numerically analyzed at transition and steady-state conditions. The computational simulation was carried out using the finite difference technique [24,29,30]. The simulation results qualitatively explained and confirmed the experimentally observed effect of the synergistic substrates conversion on the biosensor response [13].

2. Mathematical Model

We consider the following kinetic scheme used for the determination of synergistic substrates [13]:

$$E_{ox} + R \xrightarrow{k_1} E_{red} + P \tag{1a}$$

$$E_{red} + S_1 \xrightarrow{k_2} E_{ox} + P_1 \tag{1b}$$

$$E_{red} + S_2 \xrightarrow{k_3} E_{ox} + P_2 \tag{1c}$$

$$S_1 + P_2 \xrightarrow{k_4} P_1 + S_2 \tag{1d}$$

$$P_1 \longrightarrow S_1 + n_1 e^- \tag{1e}$$

$$P_2 \longrightarrow S_2 + n_2 e^- \tag{1f}$$

where E_{ox} and E_{red} stand for oxidized and reduced enzyme forms, respectively, R is the enzyme reducer, S_1 and S_2 are the substrates, P, P_1 and P_2 are the products of the reactions, k_1, k_2, k_3, k_4 are the reaction rate constants, and n_1, n_2 are the numbers of electrons involved in a charge transfer at the electrode surface in reactions (1e) and (1f), respectively.

The reactions (1a) and (1b) may be considered as the reduction of a low reactive electron acceptor S_1 by R and catalyzed by the enzyme. In the reaction (1a), the enzyme is reduced by the reducer R, and an intermediate form of enzyme (E_{red}) is formed. In the reaction (1b), the electron acceptor S_1 is reduced by the E_{red}, the product P_1 is formed and enzyme molecules regain their primary oxidized form E_{ox}.

When the high reactive electron acceptor S_2 is introduced, two more reactions, (1c) and (1d), start. The reaction (1c) represents the enzyme oxidation by the high reactive electron acceptor S_2. The reaction (1d) is called a cross reaction. In the latter reaction, the substrate S_1 oxidizes the product P_2 and regenerates the substrate S_2. This reaction also produces the product P_1.

Reactions (1e) and (1f) are electrochemical reactions that take place on the biosensor electrode. Both reactions are assumed fast and irreversible due to the high electrode potential.

$[\mathrm{Fe(CN)_6}]^{3-}$ ion may be employed as the low reactive electron acceptor S_1 [13,15]. In this case, $[\mathrm{Fe(CN)_6}]^{4-}$ ion would be the reaction product P_1. Cation radicals of 1-(N,N-dimethylamino)-4-(4-morpholino)benzene, 5,10-dihydro-5,10-dimethylphenazine, phenoxazine-10-propionic acid or phenothiazine-10-propionic acid may be used as high reactive electron acceptors (S_2). The reduced forms of those substances would be considered as the corresponding products (P_2) [13].

During the physical experiment [13], the substrate S_2 was introduced into the bulk solution at the moment when the steady-state response to the substrate S_1 was established. The thickness of the diffusion layer was controlled by the rotating magnetic bar and it was estimated using the rotating disk electrode.

2.1. Biosensor Structure

The biosensor is considered as an electrode with a relatively thin layer of enzyme solution trapped on the surface of the electrode by applying a dialysis membrane [13]. The biosensor model involves four regions: the enzyme layer where the enzymatic and chemical reactions as well as the mass transport by diffusion take place, a dialysis membrane, a diffusion limiting region where only chemical reactions as well as the mass transport by diffusion take place, and a convective region where the analyte concentration is maintained constant, see Figure 1. Assuming a homogeneous distribution of the enzyme in the enzyme layer of the uniform thickness and symmetrical geometry of the dialysis membrane leads to the mathematical model of the biosensor action defined in a one-dimensional-in-space domain [23,24].
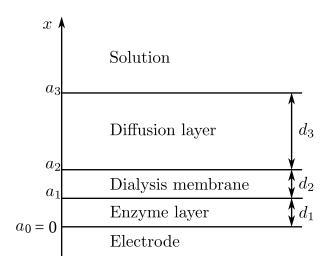
Figure 1. Principal structure of a biosensor.

Let us define d_1, d_2 and d_3 as the thicknesses of the enzyme, dialysis membrane and diffusion layers, respectively. We will also need values representing the distances between the electrode surface and the boundaries of the regions. Let a_1, a_2 and a_3 be the distances between the electrode surface and one of those boundaries shown in Figure 1.

The diffusion layer $(a_2 < x < a_3)$ may be treated as the Nernst diffusion layer [29]. According to the Nernst approach a layer of thickness d_3 remains unchanged with time. It was assumed that away from it the solution is uniform in concentration.

2.2. Governing Equations

The governing equations for a chemical reaction network can be formulated by the law of mass action [11,21]. Coupling reactions in the enzyme layer with the one-dimensional-in-space diffusion, described by the Fick's second law, leads to the following equations of the reaction–diffusion type $(0 < x < a_1, t > 0)$:

$$\frac{\partial e_{ox}}{\partial t} = -k_1 e_{ox} r_1 + k_2 e_{red} s_{11} + k_3 e_{red} s_{21} \tag{2a}$$

$$\frac{\partial e_{red}}{\partial t} = k_1 e_{ox} r_1 - k_2 e_{red} s_{11} - k_3 e_{red} s_{21} \tag{2b}$$

$$\frac{\partial r_1}{\partial t} = D_{R1} \frac{\partial^2 r_1}{\partial x^2} - k_1 e_{ox} r_1 \tag{2c}$$

$$\frac{\partial s_{11}}{\partial t} = D_{S_11} \frac{\partial^2 s_{11}}{\partial x^2} - k_2 e_{red} s_{11} - k_4 s_{11} p_{21} \tag{2d}$$

$$\frac{\partial s_{21}}{\partial t} = D_{S_21} \frac{\partial^2 s_{21}}{\partial x^2} - k_3 e_{red} s_{21} + k_4 s_{11} p_{21} \tag{2e}$$

$$\frac{\partial p_{11}}{\partial t} = D_{P_11} \frac{\partial^2 p_{11}}{\partial x^2} + k_2 e_{red} s_{11} + k_4 s_{11} p_{21} \tag{2f}$$

$$\frac{\partial p_{21}}{\partial t} = D_{P_21} \frac{\partial^2 p_{21}}{\partial x^2} + k_3 e_{red} s_{21} - k_4 s_{11} p_{21} \tag{2g}$$

where x stands for space, t is time, $e_{ox}(x,t)$ and $e_{red}(x,t)$ correspond to concentrations of oxidized (E_{ox}) and reduced (E_{red}) enzyme, respectively; $s_{11}(x,t)$ and $s_{21}(x,t)$ $(p_{11}(x,t)$ and $p_{21}(x,t))$ are the

concentrations of substrates (products) in the enzyme layer; $r_1(x,t)$ is the reducer concentration in the enzyme layer, and D_{R1}, D_{S_11}, D_{S_21}, D_{P_11}, D_{P_21} are the diffusion coefficients of the corresponding substances defined by the subscript. In the definition of the concentrations and diffusion coefficients, here and later in this paper the last numeric subscript label denotes the region of the model, particularly, 1 stands for the enzyme layer. The molecules of both enzyme forms, E_{ox} and E_{red}, are considered as immobilized, and therefore there are no diffusion terms in the corresponding equations.

The product P does not act as a reactant in any reaction, so its concentration is not used in any further calculations. Therefore, equation system (2) contains no equation for the product P.

No enzyme molecules appear in the dialysis membrane as well as in the diffusion layer. Only the reaction (1d) as well as the mass transport by diffusion of the reducer, substrates and products take place in these two regions. The governing equations for both these layers are represented as follows ($a_{i-1} < x < a_i$, $t > 0$, $i = 2, 3$):

$$\frac{\partial r_i}{\partial t} = D_{Ri}\frac{\partial^2 r_i}{\partial x^2} \tag{3a}$$

$$\frac{\partial s_{1i}}{\partial t} = D_{S_1i}\frac{\partial^2 s_{1i}}{\partial x^2} - k_4 s_{1i} p_{2i} \tag{3b}$$

$$\frac{\partial s_{2i}}{\partial t} = D_{S_2i}\frac{\partial^2 s_{2i}}{\partial x^2} + k_4 s_{1i} p_{2i} \tag{3c}$$

$$\frac{\partial p_{1i}}{\partial t} = D_{P_1i}\frac{\partial^2 p_{1i}}{\partial x^2} + k_4 s_{1i} p_{2i} \tag{3d}$$

$$\frac{\partial p_{2i}}{\partial t} = D_{P_2i}\frac{\partial^2 p_{2i}}{\partial x^2} - k_4 s_{1i} p_{2i} \tag{3e}$$

where $i = 2$ corresponds to the dialysis membrane, and $i = 3$ corresponds to the diffusion layer.

2.3. Initial Conditions

Let $x = 0$ represents the electrode surface, while $x = a_1$, $x = a_2$ and $x = a_3$ represent the boundaries between the adjacent regions as described in Section 2.1 and shown in Figure 1. The biosensor operation starts when the reducer and the substrates appear in the bulk solution. This is used in the initial conditions ($t = 0$),

$$r_1(x,0) = s_{i1}(x,0) = p_{i1}(x,0) = 0, \quad 0 \le x \le a_1, \quad i = 1,2 \tag{4a}$$

$$e_{red}(x,0) = 0, \quad e_{ox}(x,0) = e_0, \quad 0 < x < a_1 \tag{4b}$$

$$r_2(x,0) = s_{i2}(x,0) = p_{i2}(x,0) = 0, \quad a_1 \le x \le a_2, \quad i = 1,2 \tag{4c}$$

$$p_{i3}(x,0) = 0, \quad a_2 \le x \le a_3, \quad i = 1,2 \tag{4d}$$

$$r_3(x,0) = s_{i3}(x,0) = 0, \quad a_2 \le x < a_3, \quad i = 1,2 \tag{4e}$$

$$r_3(a_3,0) = r_0, \quad s_{13}(a_3,0) = s_{10} \tag{4f}$$

$$s_{23}(a_3,0) = \begin{cases} 0, & T_{S_2} > 0 \\ s_{20}, & T_{S_2} = 0 \end{cases} \tag{4g}$$

where e_0 stands for the total concentration of the enzyme in the enzyme layer ($e_0 = e_{ox}(x,t) + e_{red}(x,t)$, $\forall x, t : x \in (0, a_1), t > 0$), r_0 is the reducer concentration in the bulk solution, s_{10} and s_{20}

stand for substrate concentrations in the bulk solution, T_{S_2} is the moment of the substrate S_2 insertion into the bulk solution.

2.4. Matching Conditions

On the boundary between two regions having different diffusivities, matching conditions have to be defined ($t > 0$, $i = 1, 2$, $m = 1, 2$),

$$D_{Rm} \left.\frac{\partial r_m}{\partial x}\right|_{x=a_m} = D_{R,m+1} \left.\frac{\partial r_{m+1}}{\partial x}\right|_{x=a_m}, \qquad r_m(a_m, t) = r_{m+1}(a_m, t) \tag{5a}$$

$$D_{S_i m} \left.\frac{\partial s_{im}}{\partial x}\right|_{x=a_m} = D_{S_i,m+1} \left.\frac{\partial s_{i,m+1}}{\partial x}\right|_{x=a_m}, \qquad s_{im}(a_m, t) = s_{i,m+1}(a_m, t) \tag{5b}$$

$$D_{P_i m} \left.\frac{\partial p_{im}}{\partial x}\right|_{x=a_m} = D_{P_i,m+1} \left.\frac{\partial p_{i,m+1}}{\partial x}\right|_{x=a_m}, \qquad p_{im}(a_m, t) = p_{i,m+1}(a_m, t) \tag{5c}$$

where $m = 1$ corresponds to the boundary between the enzyme layer and the dialysis membrane, whereas $m = 2$ corresponds to the boundary between the dialysis membrane and the diffusion layer.

These conditions mean that fluxes of the reducer, substrates and products through one region are equal to the corresponding fluxes entering the surface of the neighboring region. Concentrations of the reducer, substrates and products in one region *versus* the neighboring region are assumed to be equal.

2.5. Boundary Conditions

In the bulk solution, concentrations of the reducer, substrates and products remain constant ($t > 0$),

$$r_3(a_3, t) = r_0 \tag{6a}$$

$$s_{13}(a_3, t) = s_{10} \tag{6b}$$

$$s_{23}(a_3, t) = \begin{cases} 0, & t < T_{S_2} \\ s_{20}, & t \geq T_{S_2} \end{cases} \tag{6c}$$

$$p_{i3}(a_3, t) = 0, \quad i = 1, 2 \tag{6d}$$

The reaction products P_1 and P_2 take part in the electrochemical reactions (1e) and (1f), respectively, at the electrode surface ($x = 0$). Rates of those reactions are so high that the concentrations of P_1 and P_2 at the electrode surface are permanently reduced to zero ($t > 0$) [13],

$$p_{11}(0, t) = 0 \tag{7a}$$

$$p_{21}(0, t) = 0 \tag{7b}$$

Since the reaction (1e) produces as much S_1 as it consumes P_1, the concentration flux of P_1 on the electrode surface is equal to the concentration flux of S_1 but in opposite direction. The same is also assumed for the reaction (1f) and substances S_2 and P_2. These relations are expressed by the following boundary conditions ($t > 0$):

$$D_{P_1 1} \left.\frac{\partial p_{11}}{\partial x}\right|_{x=0} = -D_{S_1 1} \left.\frac{\partial s_{11}}{\partial x}\right|_{x=0} \tag{8a}$$

$$D_{P_21} \left. \frac{\partial p_{21}}{\partial x} \right|_{x=0} = -D_{S_21} \left. \frac{\partial s_{21}}{\partial x} \right|_{x=0} \tag{8b}$$

The reducer R is electrode-inactive substance, thus its concentration flux on the electrode surface is equal to zero $(t > 0)$,

$$D_{R1} \left. \frac{\partial r_1}{\partial x} \right|_{x=0} = 0 \tag{9}$$

2.6. Biosensor Response

The measured current is usually assumed as the response of an amperometric biosensor in physical experiments. When modelling the biosensor action, due to the direct proportionality of the current to the area of the electrode surface, the current is often normalized with that area [23,31]. The biosensor current density $j(t)$ at time t was expressed explicitly from Faraday's and Fick's laws,

$$j_1(t) = n_1 F D_{P_11} \left. \frac{\partial p_{11}}{\partial x} \right|_{x=0} \tag{10a}$$

$$j_2(t) = n_2 F D_{P_21} \left. \frac{\partial p_{21}}{\partial x} \right|_{x=0} \tag{10b}$$

$$j(t) = j_1(t) + j_2(t) \tag{10c}$$

where $j_1(t)$ and $j_2(t)$ are the faradaic current densities generated by the electrochemical reactions (1e) and (1f), respectively, F is the Faraday constant, $F = 96,486 \, \text{C/mol}$.

We assume that the system approaches a steady state as $t \to \infty$,

$$j_{st} = \lim_{t \to \infty} j(t) \tag{11a}$$

$$j_{1st} = \lim_{t \to \infty} j_1(t) \tag{11b}$$

$$j_{2st} = \lim_{t \to \infty} j_2(t) \tag{11c}$$

where j_{st}, j_{1st} and j_{2st} are the steady-state biosensor current densities.

Since the current is generated due to two electrochemical reactions (1e) and (1f), it is important to investigate the influence of each of them to the overall biosensor response. The contribution of the electrochemical reaction (1e) into the overall biosensor response was expressed as the ratio of the density of the steady-state current j_{1st} to the density j_{st} of the overall steady-state current,

$$J_1 = \frac{j_{1st}}{j_{st}} \tag{12}$$

The sensitivity is also one of the most important characteristics of biosensors [1,2]. The biosensor sensitivity is usually expressed as the gradient of the biosensor current with respect to the concentration of the substrate in the bulk. Since the biosensor current as well as the substrate concentration varies even in orders of magnitude, a dimensionless expression of the sensitivity is preferable [31,32].

The biosensor based on synergistic reactions is designed to measure concentration of the substrate S_2 [13]. The dimensionless biosensor sensitivity B to the concentration of the substrate S_2 was defined as follows:

$$B(s_{20}) = \frac{\mathrm{d} j_{st}(s_{20})}{\mathrm{d} s_{20}} \times \frac{s_{20}}{j_{st}(s_{20})} \tag{13}$$

where $j_{st}(s_{20})$ is the density of the steady-state biosensor current calculated at the concentration s_{20} of the substrate S_2 in the bulk. $B(s_{20})$ denotes the biosensor sensitivity at that concentration.

The chemical signal amplification caused by a synergistic effect is another important characteristic of this type of biosensors [13]. A measure Amp of the synergistic effect was expressed as the ratio of the biosensor response to a substrate S_2-containing analyte to the response to the corresponding S_2-free analyte,

$$Amp(s_{20}) = \frac{j_{st}(s_{20})}{j_{st}(0)} \tag{14}$$

where $Amp(s_{20})$ is the dimensionless ratio of the signal amplification obtained by the insertion of the substrate S_2 of the concentration s_{20} into the buffer solution [13,22].

3. Numerical Simulation of Biosensor Action

3.1. Simulating the Biosensor Operation

Analytical solutions are not usually possible when solving non-linear partial differential equations [19,23,29]. Therefore, the biosensor action was simulated numerically. The simulation was carried out using the finite difference technique [29,30]. An explicit finite difference scheme was built on a uniform discrete grid with 200 points in space direction for each modelled layer corresponding to a certain time moment. The simulator has been programmed by authors in C programming language [33].

In the numerical simulation, the biosensor response time was assumed as the time when the change of the biosensor current remains very small during a relatively long term. A special dimensionless decay rate ε was used,

$$t_r = \min_{j(t)>0} \left\{ t : \frac{t}{j(t)} \left| \frac{\mathrm{d}j(t)}{\mathrm{d}t} \right| < \varepsilon \right\}, \quad j(t_r) \approx j_{st} \tag{15}$$

where t_r is the biosensor response time. The decay rate value $\varepsilon = 10^{-3}$ was used in calculations.

The following values of the model parameters were constant in all numerical simulations, unless stated otherwise [13]:
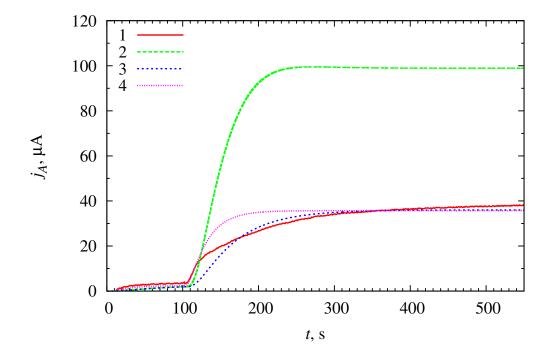
$$k_1 = 1.25 \times 10^4 \, \mathrm{M}^{-1}\,\mathrm{s}^{-1}, \quad k_2 = 1.2 \times 10^2 \, \mathrm{M}^{-1}\,\mathrm{s}^{-1}$$
$$k_3 = 1.4 \times 10^6 \, \mathrm{M}^{-1}\,\mathrm{s}^{-1}, \quad k_4 = 1.4 \times 10^6 \, \mathrm{M}^{-1}\,\mathrm{s}^{-1}$$
$$e_0 = 0.04 \, \mathrm{mM}, \quad s_{10} = 8 \, \mathrm{mM}, \quad r_0 = 40 \, \mathrm{mM}$$
$$D_{R1} = D_{S_i1} = D_{P_i1} = 3.15 \times 10^{-6} \, \mathrm{cm}^2/\mathrm{s}, \quad i = 1, 2$$
$$D_{R2} = D_{S_i2} = D_{P_i2} = 4.2 \times 10^{-7} \, \mathrm{cm}^2/\mathrm{s}, \quad i = 1, 2$$
$$D_{R3} = D_{S_i3} = D_{P_i3} = 6.3 \times 10^{-6} \, \mathrm{cm}^2/\mathrm{s}, \quad i = 1, 2$$
$$d_1 = 23.3 \, \mathrm{\mu m}, \quad d_2 = 18.6 \, \mathrm{\mu m}$$
$$n_1 = n_2 = 1$$

3.2. Experimental Validation

The numerical solution of the model (2)–(10) was compared with the experimental data of the research conducted by one of the authors [13]. The results are depicted in Figure 2. The experimental data were

shifted by $-30\,\text{s}$ in time axis and by $-1.9\,\mu\text{A}$ in current axis [13]. The correction in time axis was applied in order to coincide the addition of reducer R (glucose in this particular case) into the bulk solution at the moment $t = 0$. The correction in current axis was applied in order to eliminate the background current influence to the overall biosensor response.

Figure 2. Model validation with experimental data; (1) experimental data, (2)–(4) simulation results. Simulation was carried out at two reaction rate constants (k_3) of the reaction (1c) ($1.4 \times 10^6\,\text{M}^{-1}\,\text{s}^{-1}$ (2) and $0.35 \times 10^6\,\text{M}^{-1}\,\text{s}^{-1}$ (3, 4)) and at two thicknesses (d_3) of the diffusion layer ($223\,\mu\text{m}$ (2, 3) and $116.5\,\mu\text{m}$ (4)); $s_{20} = 39\,\mu\text{M}$.

During physical experiment, the substrate S_2 was added into the bulk solution at the moment $t = 130\,\text{s}$ which corresponds to $t = 100\,\text{s}$ in the simulations. Thus $T_{S_2} = 100\,\text{s}$ value was used in the numerical simulations. Having simulated density j of the biosensor current, the biosensor current j_A was calculated by multiplying the density by the area A of the electrode surface,

$$j_A = jA \tag{16}$$

In the physical experiment, the electrode with the surface area of $A = 0.3\,\text{cm}^2$ was used [13].

The curve 2 in Figure 2 corresponds to the simulation carried out at the parameters equal to the parameters of the physical experiment [13]. The relative difference between the numerical solution and the experiment data at the moment T_{S_2} (before insertion of S_2) is about 14%. This indicates that mathematical model quite accurately reflects the physical experiment. However, after the insertion of S_2, the accuracy deteriorates. The simulated steady-state current is about 2.5 times higher than the experimental one (Figure 2). This indicates that experiment is really more complex than as defined by the mathematical model. Presumably, the reaction of the reduced enzyme with oxygen, which was unforeseen in the mathematical modelling, is a main factor determining this difference [13]. The difference may be also caused by the limited stability of oxidized heterocyclic compounds and some external diffusion limitation of substrates [13].

The curves 3 and 4 of Figure 2 demonstrate that simulation results may be fitted with the experimental ones by varying the value of the reaction rate constant k_3 and the diffusion layer thickness d_3. However the measured values of the parameters will be used in this paper in further numerical simulations.

Despite this inadequacy with the experiment, the model (2)–(10) seems to be suitable for investigating the kinetic peculiarities and optimizing the configuration of biosensors utilizing the synergistic effect of substrates.

3.3. Simulating the Synergistic Effect

The understanding the nature of the synergistic effect is of crucial importance for preparation of highly sensitive biosensors [13,15,26]. For a kinetic analysis of the biosensor operation, let us introduce $\bar{v}_1$, $\bar{v}_2$, $\bar{v}_3$, $\bar{v}_4$ as the average rates of the reactions $(1a)$, $(1b)$, $(1c)$, $(1d)$ taking place in the enzyme layer,

$$\bar{v}_1 = k_1 \bar{e}_{ox} \bar{r} \tag{17a}$$

$$\bar{v}_2 = k_2 \bar{e}_{red} \bar{s}_1 \tag{17b}$$

$$\bar{v}_3 = k_3 \bar{e}_{red} \bar{s}_2 \tag{17c}$$

$$\bar{v}_4 = k_4 \bar{s}_1 \bar{p}_2 \tag{17d}$$

where $\bar{r}$, $\bar{s}_1$, $\bar{s}_2$, $\bar{p}_1$, $\bar{p}_2$, $\bar{e}_{ox}$ and $\bar{e}_{red}$ stand for the average concentrations of R, S_1, S_2, P_1, P_2, E_{ox} and E_{red} in the enzyme layer.

Figures 3 and 4 show how the synergistic effect occurs. The biosensor parameters were kept the same as in Figure 2.

Figure 3. Average concentrations $\bar{r}$ (1), $\bar{s}_1$ (2), $\bar{s}_2$ (3), $\bar{p}_1$ (4), $\bar{p}_2$ (5), $\bar{e}_{ox}$ (6) and $\bar{e}_{red}$ (7).
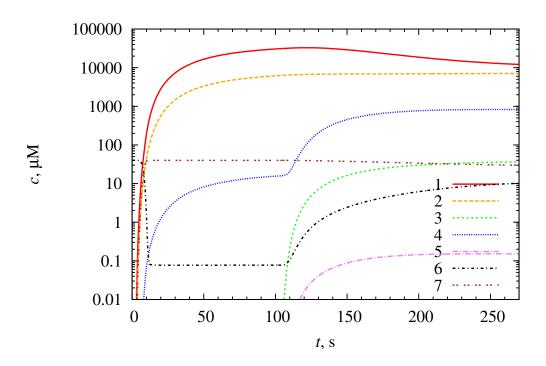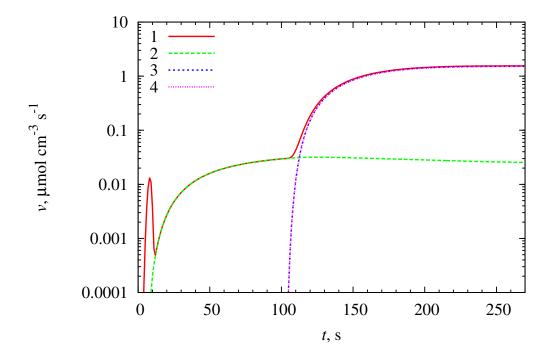
Figure 4. Average rates $\bar{v}_1$ (1), $\bar{v}_2$ (2), $\bar{v}_3$ (3), $\bar{v}_4$ (4) of the reactions (1a)–(1d) taking place in the enzyme layer (curves 3 and 4 coincide).

When S_2 is introduced into the bulk solution, a fast reaction (1c) starts, and a large amount of E_{ox} and P_2 molecules are produced (see Figure 3). In the meantime the increased concentration of E_{ox} initiates an increase in the rate of the reaction (1a), molecules of P_2 start to react with S_1 in reaction (1d) (see Figure 4). A decrease of the reducer R concentration is the second indication of the increase in the reaction (1a) rate as the reaction consumes more reactant molecules (see Figure 3). The reactions (1a) and (1c) are very strongly interrelated because E_{ox} is the product of reaction (1c), and at the same time it is the reactant of the reaction (1a) and vice versa with E_{red} molecule. Similar situation appears with the reactions (1c) and (1d) (molecules of P_2 and S_2).

The rate of the reaction (1c) is controlled by the concentration of S_2. Reactions (1a) and (1d) are accelerated by the reaction (1c) and their rates tend to reach the rate of the reaction (1c). Hence the rates of reactions (1a), (1c) and (1d) are approximately equal during almost all the time of biosensor operation as seen in Figure 4. The rate of the reaction (1b) remains almost unaffected.

The reactions (1b) and (1d) produce the product P_1 which is responsible for the biosensor current. Since the rate of the reaction (1b) remains almost unchanged and the rate of the reaction (1d) is greater than the rate of reaction (1b) by two orders of magnitude, the biosensor response is also increased by two orders of magnitude. In other words, the signal is amplified chemically. This is the desirable outcome of synergistic effect in this type of biosensors [13].
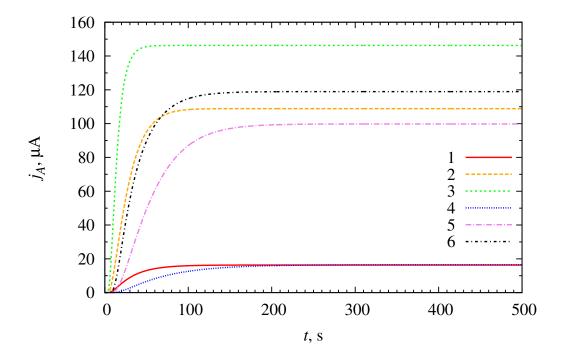
If the synergistic effect would not occur during the biosensor operation, that would mean that biosensor signal is not chemically amplified. A biosensor with no chemical amplification could be too weak for reliable measurement. That could mean the narrower range of biosensor application because biosensor would only work at relatively high concentrations of substrate. So, it is important to choose the correct biosensor parameters that support the occurrence of the synergistic effect.

The law of mass conservation was applied for an additional validation of the numerical solution of the initial boundary value problem Equations (2)–(9). Since no mass transport of the enzyme takes place in the enzyme layer, the equality $e_{ox}(x,t) + e_{red}(x,t) = e_0$ holds for $\forall x \in [0, a_1]$ and $\forall t \geq 0$. At the steady-state conditions when $\partial s_{im}/\partial t = \partial p_{im}/\partial t = 0$, the equality $s_{im}(x,t) + p_{im}(x,t) = s_{i0}$ holds for $\forall x \in [a_{m-1}, a_m]$ and $t \rightarrow \infty$, $i = 1, 2$, $m = 1, 2, 3$. A fulfillment of these conditions can be observed in Figure 3 (please note that concentrations are provided in a logarithmic scale).

3.4. Dynamics of Biosensor Current

Figure 5 shows the dynamics of the biosensor current j_A simulated at two thicknesses (d_3) of the diffusion layer and three concentrations (s_{20}) of the substrate S_2. For simplicity, here and below, the substrate S_2 is introduced in the bulk solution in the beginning of the experiments ($T_{S_2} = 0\,\text{s}$).

Figure 5. The evolution of the biosensor current j_A at different thicknesses (d_3) of the diffusion layer ($116.5\,\mu\text{m}$ (1, 2, 3) and $233\,\mu\text{m}$ (4, 5, 6)) and concentrations (s_{20}) of the substrate S_2 ($4\,\mu\text{M}$ (1, 4), $40\,\mu\text{M}$ (2, 5) and $400\,\mu\text{M}$ (3, 6).

At low substrate concentration ($s_{20} = 4\,\mu\text{M}$) the steady-state current of the biosensor is not influenced by the thickness d_3 of the diffusion layer. However at this concentration, a change in the thickness of the diffusion layer slightly changes the curvature of "current *vs.* time" curve and the biosensor with thinner diffusion layer reaches the steady state earlier. This is also correct in cases of higher substrate concentrations ($s_{20} = 40\,\mu\text{M}$, $s_{20} = 400\,\mu\text{M}$).
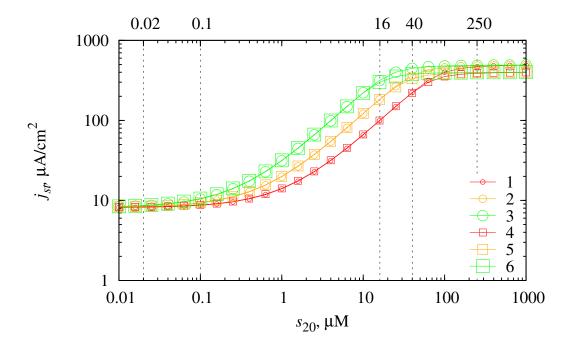
From the curves depicted in Figure 5 one can also observe another very important relationship: the steady-state current directly depends on the concentration s_{20} of the substrate S_2 in the bulk solution. At higher substrate concentrations ($s_{20} = 40\,\mu\text{M}$, $s_{20} = 400\,\mu\text{M}$) it is also observable that steady-state current depends inversely on the thickness d_3 of the diffusion layer. Intensity of the solution stirring plays important role when working with solutions of high concentration of the substrate.

4. Results and Discussion

4.1. Biosensor Response vs. Substrates Concentrations

The dependence of the steady-state biosensor current on the concentration s_{20} of the substrate S_2 was investigated at different diffusion layer thicknesses d_3 as well as at different values of the reaction rate constant k_3. The results of the numerical simulations are depicted in Figure 6.

Figure 6. The dependence of the steady-state current density j_{st} on the substrate concentration s_{20} at two thicknesses (d_3) of the diffusion layer ($116.5\,\mu\text{m}$ (1, 2, 3) and $233\,\mu\text{m}$ (4, 5, 6)) and three reaction rate constants (k_3) of the reaction (1c) ($7 \times 10^5\,\text{M}^{-1}\,\text{s}^{-1}$ (1, 4), $1.4 \times 10^6\,\text{M}^{-1}\,\text{s}^{-1}$ (2, 5) and $2.8 \times 10^6\,\text{M}^{-1}\,\text{s}^{-1}$ (3, 6)).

The biosensor may reliably measure the concentration of substrate S_2 at the range of concentrations where the biosensor response is dependent on the concentration s_{20} but not dependent on the diffusion layer thickness d_3. As one can observe from Figure 6 this range depends on the reaction rate constant k_3. The lower boundary of this range varies from $s_{20} \approx 0.02\,\mu\text{M}$ when k_3 is relatively high (curves 3, 6) to $s_{20} \approx 0.1\,\mu\text{M}$ when k_3 is relatively low (curves 1, 4). The upper boundary of this range varies from $s_{20} \approx 16\,\mu\text{M}$ when k_3 is relatively high (curves 3, 6) to $s_{20} \approx 40\,\mu\text{M}$ when k_3 is relatively low (curves 1, 4). At the concentrations $s_{20} \gtrsim 250\,\mu\text{M}$ the biosensor response is not influenced by the concentration of the substrate S_2.

To investigate the dependence of the biosensor sensitivity on the substrate concentration, the biosensor response was simulated at the same values of the diffusion layer thickness d_3 and the reaction rate constant k_3 as in Figure 6. The calculation results are depicted in Figure 7.

Figure 7. The dependence of the biosensor sensitivity B on the substrate concentration s_{20}. Values of all parameters are the same as in Figure 6.
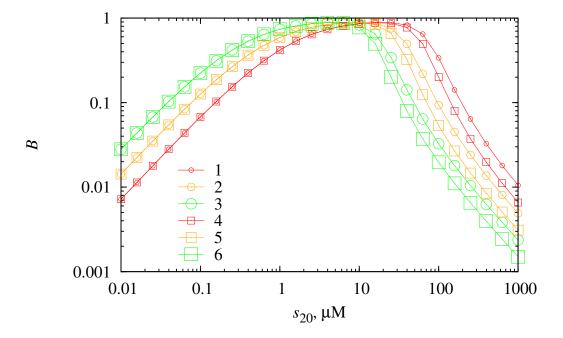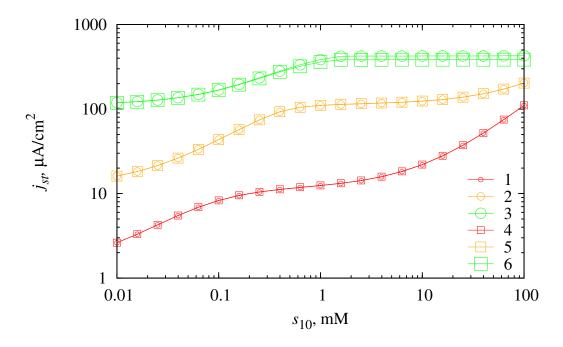

Figure 8. The dependence of the steady-state current density j_{st} on the substrate concentration s_{10} at two thicknesses (d_3) of the diffusion layer ($116.5\,\mu\text{m}$ (1, 2, 3) and $233\,\mu\text{m}$ (4, 5, 6)) and three concentrations (s_{20}) of the substrate S_2 ($1\,\mu\text{M}$ (1, 4), $10\,\mu\text{M}$ (2, 5) and $100\,\mu\text{M}$ (3, 6)).

As one can observe from Figure 7, the biosensor shows the highest values of the sensitivity when the concentration of the substrate S_2 is moderate ($1\,\mu\text{M} \leq s_{20} \leq 10\,\mu\text{M}$). At low substrate S_2 concentrations

$(0.01\,\mu\text{M} \leq s_{20} < 1\,\mu\text{M})$ as well as at high concentrations of S_2 $(10\,\mu\text{M} < s_{20} \leq 1,000\,\mu\text{M})$ biosensor exhibits poor sensitivity.

At low substrate concentrations, a higher k_3 yields a higher biosensor sensitivity, whereas the thickness d_3 of the diffusion layer does not influence the biosensor response at this concentration range. At high substrate concentrations, k_3 has the opposite effect on the biosensor sensitivity compared with a low substrate concentration range. A higher k_3 yields a lower biosensor sensitivity. At this concentration range, the thickness d_3 of the diffusion layer does influence the biosensor sensitivity. A thicker diffusion layer diminishes the value of biosensor sensitivity.

Although this type biosensors are designed to measure the concentration s_{20} of the substrate S_2, it is also important to investigate the biosensor response dependency on the concentration s_{10} of the substrate S_1 in order to optimize the biosensors. The dependence of the steady-state biosensor current j_{st} on the concentration s_{10} was investigated at different values of diffusion layer thickness d_3 as well as at different concentrations (s_{20}) of the substrate S_2. The simulation results are depicted in Figure 8.

As we can observe from the curves in Figure 8, the biosensor response directly depends on the concentration s_{10}. In cases of low and moderate substrate concentrations of S_2, this dependency holds through the whole range of investigated s_{10} concentrations. At high concentrations of S_2 ($s_{20} = 100\,\mu\text{M}$), this dependency is valid only for low concentrations of S_1 ($s_{10} < 1\,\text{mM}$). At high concentrations of S_1 ($s_{10} > 1\,\text{mM}$) the biosensor response becomes practically insensitive to the change of s_{10}.

The thickness d_3 of the diffusion layer has no noticeable influence on the biosensor response at the majority of the biosensor parameters investigated. Only at high concentrations of S_1 and high concentrations of S_2 the effect of the diffusion layer thickness becomes noticeable.

4.2. The Composition of Biosensor Response

The biosensor response is determined by two electrochemical reactions (1e) and (1f). It is important to understand the role of each process at certain values of the biosensor parameters.

The dependence of the biosensor response composition on the reaction rate constant k_4 was investigated at different diffusion layer thicknesses (d_3) as well as at different values of the substrate concentration s_{20}. Results of the numerical simulation are depicted in Figure 9.

As one can see in Figure 9, the ratio J_1 of the density j_{1st} of the steady-state current generated by the electrochemical reactions (1e) to the density j_{st} of the overall steady-state current directly depends on the reaction rate constant k_4. This can be explained by the reaction (1d). The faster the reaction (1d) the more P_2 consumes, and molecules of P_2 do not reach electrode surface.

At low s_{20} concentrations, a value of k_4 only slightly influences the composition of the biosensor response (curves 1 and 4). The biosensor response is almost entirely generated by the faradaic process (1e) at such concentrations of S_2. As one can see from the reaction scheme (1), a low concentration of S_2 directly cause a low concentration of P_2. However at a high concentration s_{20} of S_2, a value of the reaction rate constant k_4 makes a major impact on the composition of the biosensor response. When k_4 is small enough, the ratio J_1 is less than 0.5, *i.e.*, the main part of the biosensor response is generated by the faradaic process (1f).

Figure 9. The dependence of the ratio J_1 on the reaction rate k_4 at two thicknesses (d_3) of the diffusion layer (116.5 μm (1, 2, 3) and 233 μm (4, 5, 6)) and three concentrations (s_{20}) of the substrate S_2 (0.1 μM (1, 4), 10 μM (2, 5) and 1, 000 μM (3, 6)).
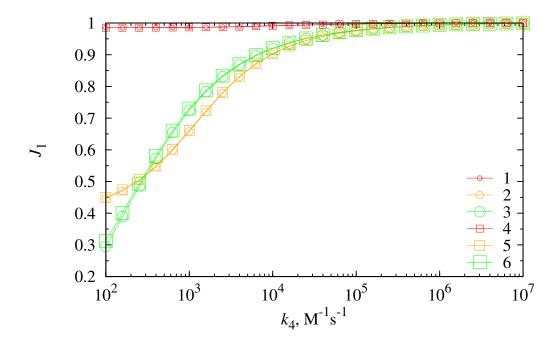

Figure 9 also shows that the thickness d_3 of the diffusion layer only slightly influences the composition of the biosensor response.

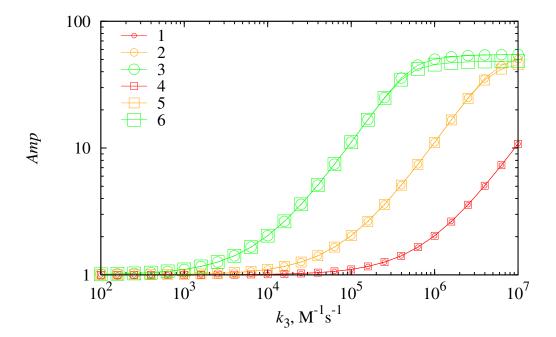*4.3. The Role of Substrates Synergistic Conversion in the Biosensor Response*

The synergistic effect was analyzed with respect to the chemical amplification *Amp*. The dependence of the chemical amplification on the reaction rate constant k_3 was investigated at different diffusion layer thicknesses (d_3) as well as at different values of the substrate concentration s_{20}. Results of the numerical simulation are depicted in Figure 10.

The direct influence of the reaction rate constant k_3 on the *Amp* is the main dependency that can be observed in Figure 10. At a higher rate constant (k_3) of the biochemical reaction (1c) more molecules of P_2 are produced. Because of this, the rate of the reaction (1d) increases, and eventually the amount of P_1 also increases. Product P_1 is the main generator of the current as was shown in the Section 4.2.

As one can also see in Figure 10, a higher concentration s_{20} of S_2 corresponds to a higher chemical amplification *Amp*. At low values of k_3 ($k_3 < 10^3 \, \mathrm{M}^{-1} \, \mathrm{s}^{-1}$) this effect is rather weak, whereas at moderate values of k_3 (from 10^4 to $10^6 \, \mathrm{M}^{-1} \, \mathrm{s}^{-1}$) this effect is strongly expressed. However, at high values of the reaction rate constant k_3 ($k_3 > 10^7 \, \mathrm{M}^{-1} \, \mathrm{s}^{-1}$) this effect noticeably diminishes again. A positive influence of s_{20} on the amplification can be explained by the increase of the rate of reaction (1c) that is caused by the increase of the concentration of one of the reactants. At low values of k_3 this is not so obvious because the increase in the reactant concentration does not counterweigh low values of k_3. At high values of k_3 the system arrives at the point where the chemical amplification *Amp* is not dependent

on the reaction rate constant k_3. The influence of the diffusion layer thickness d_3 appears noticeable only at high values of k_3.

Figure 10. The dependence of the chemical amplification Amp on the reaction rate constant k_3 at two thicknesses (d_3) of the diffusion layer (116.5 µm (1, 2, 3) and 233 µm (4, 5, 6)) and three concentrations (s_{20}) of S_2 (1 µM (1, 4), 10 µM (2, 5) and 100 µM (3, 6)).
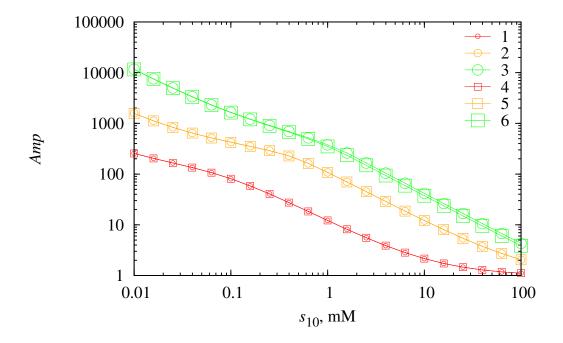

Similar limitations of the rate of the synergistic process have been also observed experimentally using glucose oxidase biosensors utilizing the synergistic substrates conversion [13].

The amplification of the biosensor current was also investigated with respect to the substrate S_1 concentration. Numerical experiments were conducted at different diffusion layer thicknesses (d_3) as well as at different concentrations (s_{20}). The results of the numerical simulation are depicted in Figure 11.

As one can see in Figure 11 the biosensor exhibits the highest values of the chemical signal amplification Amp at low concentrations of substrate S_1 and the lowest values of Amp at high values of s_{10}. So, the influence of s_{10} on the biosensor response that was observed in Figure 8 is diminished by the chemical amplification, because the magnitude of the amplification buffers the impact of the substrate S_1 concentration change. When the concentration s_{10} is low, the response of the biosensor is highly amplified by the synergistic effect and vice versa in the case of high s_{10}.

The thickness of the diffusion layer only slightly influences the chemical amplification throughout the range of the concentration s_{10} that was used in this investigation. A slight influence of the diffusion layer thickness d_3 is observed only in the case of high concentrations of both substrates, S_1 and S_2.

Figure 11. The dependence of the chemical amplification Amp on the substrate concentration s_{10} at two thicknesses (d_3) of the diffusion layer ($116.5\,\mu m$ (1, 2, 3) and $233\,\mu m$ (4, 5, 6)) and three concentrations (s_{20}) of the substrate S_2 ($1\,\mu M$ (1, 4), $10\,\mu M$ (2, 5) and $100\,\mu M$ (3, 6)).

5. Conclusions

The developed mathematical model (2)–(10) is suitable for the modelling of an amperometric biosensor with synergistic substrates conversion. The model can be used as a tool for the biosensor optimization prior to the development stage of an actual biosensor.

The investigation of the biosensor response showed that the range of concentrations, where the biosensor reliably operates, depends on the reaction rate constant k_3. In cases when k_3 is lower the biosensor may be used to measure higher concentrations s_{20}. In cases when k_3 is higher the biosensor may be used to measure lower concentrations s_{20} (Figure 6).

The biosensor has the highest sensitivity at moderate concentrations of the substrate S_2 (Figure 7). At low and high concentrations of S_2, the biosensor sensitivity is quite low.

The biosensor response is directly dependent on the concentration s_{10} of the substrate S_1. Low and moderate concentrations of S_1 are preferable, because at these concentrations the biosensor response is practically independent from the diffusion layer thickness (Figure 8).

The biosensor response almost entirely depends on the electrochemical reaction (1e) (Figure 9). The electrochemical reaction (1f) may generate a significant current only in cases when the reaction rate constant of cross reaction (1d) is low and the concentration s_{20} of S_2 is moderate or high (Figure 9).

The biosensor exhibits the highest values of the chemical amplification in cases when the reaction rate constant k_3 as well as the concentration s_{20} are the high (Figure 10). The diffusion has a minor effect on the rate Amp of the chemical amplification. A thicker diffusion layer weakens the chemical amplification only at high values of the reaction rate constant k_3 and high concentrations of S_2. The

amplification ratio Amp inversely depends on the concentration s_{10} of the substrate S_1 (Figure 11). This effect is somewhat opposite to the s_{10} effect on the biosensor response.

To prove conclusions made the physical experiments are running using glucose dehydrogenase as well as laccase-based biosensors with different configurations. A more precise computational model implying the reaction of the reduced enzyme with oxygen in addition to the reactions (1e) and (1f) is now under development for a more accurate simulation of the biosensor action.

Acknowledgements

References

1. Turner, A.P.F.; Karube, I.; Wilson, G.S. *Biosensors: Fundamentals and Applications*; Oxford University Press: Oxford, UK, 1987; p. 770.

2. Scheller, F.W.; Schubert, F. *Biosensors*; Elsevier Science: Amsterdam, The Netherlands, 1992; p. 360.

3. Malhotra, B.D.; Turner, A. *Advances in Biosensors: Perspectives in Biosensors*; Elsevier Science: Amsterdam, The Netherlands, 2003; Volume 5.

4. Chaubey, A.; Malhotra, B. Mediated biosensors. *Biosens. Bioelectron.* **2002**, *17*, 441–456.

5. Ronkainen, N.J.; Halsall, H.B.; Heineman, W.R. Electrochemical biosensors. *Chem. Soc. Rev.* **2010**, *39*, 1747–1763.

6. Rogers, K.R. Biosensors for environmental applications. *Biosens. Bioelectron.* **1995**, *10*, 533–541.

7. Scheller, F.W.; Schubert, F.; Fedrowitz, J. *Practical Applications*; Birkhäuser: Basel, Switzerland, 1997; Volume 2, p. 175.

8. Liang, J.F.; Li, Y.T.; Yang, V.C. Biomedical application of immobilized enzymes. *J. Pharm. Sci.* **2000**, *89*, 979–990.

9. Yu, D.; Blankert, B.; Vire, J.C.; Kauffmann, J.M. Biosensors in drug discovery and drug analysis. *Anal. Lett.* **2005**, *38*, 1687–1701.

10. Yoo, E.H.; Lee, S.Y. Glucose biosensors: An overview of use in clinical practice. *Sensors* **2010**, *10*, 4558–4576.

11. Gutfreund, H. *Kinetics for the Life Sciences*; Cambridge University Press: Cambridge, UK, 1995; p. 346.

12. Kulys, J.; Tetianec, L.; Bratkovskaja, I. Pyrroloquinoline quinone-dependent carbohydrate dehydrogenase: Activity enhancement and the role of artificial electron acceptors. *Biotechnol. J.* **2010**, *5*, 822–828.

13. Kulys, J.; Tetianec, L. Synergistic substrates determination with biosensors. *Biosens. Bioelectron.* **2005**, *21*, 152–158.

14. Bratkovskaja, I.; Ivanec, R.; Kulys, J. Mediator-assisted laccase-catalyzed oxidation of 4-hydroxybiphenyl. *Biochemistry (Moscow)* **2006**, *71*, 550–554.

15. Kulys, J.; Vidziunaite, R. Laccase based synergistic electrocatalytical system. *Electroanalysis* **2009**, *21*, 2228–2233.

16. Corcuera, J.I.R.D.; Cavalieri, R.P.; Powers, J.R.; Tang, J. Amperometric Enzyme Biosensor Optimization Using Mathematical Modeling. In *Proceedings of the 2004 ASAE/Csae Annual International Meeting*, Ottawa, ON, Canada, 1–4 August 2004.

17. Ferreira, L.S.; Souza, M.B.D.; Trierweiler, J.O.; Broxtermann, O.; Folly, R.O.M.; Hitzmann, B. Aspects concerning the use of biosensors for process control: Experimental and simulation investigations. *Comput. Chem. Eng.* **2003**, *27*, 1165–1173.

18. Mell, L.D.; Maloy, J.T. A model for the amperometric enzyme electrode obtained through digital simulation and applied to the immobilized glucose oxidase system. *Anal. Chem.* **1975**, *47*, 299–307.

19. Kernevez, J.P. *Studies in Mathematics and Its Applications*; Elsevier Science: Amsterdam, The Netherlands, 1980; Volume 10.

20. Kulys, J. The development of new analytical systems based on biocatalysts. *Anal. Lett.* **1981**, *14*, 377–397.

21. Bartlett, P.N.; Whitaker, R.G. Electrochemical imobilisation of enzymes: Part 1. Theory. *J. Electroanal. Chem.* **1987**, *224*, 27–35.

22. Baronas, R.; Kulys, J.; Ivanauskas, F. Mathematical model of the biosensors acting in a trigger mode. *Sensors* **2004**, *4*, 20–36.

23. Schulmeister, T. Mathematical modelling of the dynamic behaviour of amperometric enzyme electrodes. *Sel. Electrode Rev.* **1990**, *12*, 203–260.

24. Baronas, R.; Ivanauskas, F.; Kulys, J. *Mathematical Modeling of Biosensors*; Springer: Dordrecht, The Netherlands, 2010; Volume 9, p. 353.

25. Kulys, J. Kinetics of biocatalytical synergistic reactions. *Nonlinear Anal. Model. Control* **2005**, *10*, 223–233.

26. Kulys, J.; Dapkūnas, Z. The effectiveness of synergistic enzymatic reaction with limited mediator stability. *Nonlinear Anal. Model. Control* **2007**, *12*, 495–501.

27. Gaidamauskaite, E.; Baronas, R.; Kulys, J. Modelling synergistic action of laccase-based biosensor utilizing simultaneous substrates conversion. *J. Math. Chem* **2011**, *49*, 1573–1586.

28. Aris, R. *The Theory of the Steady State*; Clarendon Press: Oxford, UK, 1975; Volume 1, p. 444.

29. Britz, D. *Digital Simulation in Electrochemistry*, 3rd ed.; Springer: Berlin, Heidelberg, Germany, 2005; p. 338.

30. Samarskii, A.A. *The Theory of Difference Schemes*; Marcel Dekker: New York, NY, USA, 2001; p. 761.

31. Baronas, R.; Kulys, J. Modelling amperometric biosensors based on chemically modified electrodes. *Sensors* **2008**, *8*, 4800–4820.

32. Šimelevičius, D.; Baronas, R. Computational modelling of amperometric biosensors in the case of substrate and product inhibition. *J. Math. Chem* **2010**, *47*, 430–445.

33. Press, W.H.; Teukolsky, S.A.; Vetterling, W.T.; Flannery, B.P. *Numerical Recipes in C: The Art of Scientific Computing*, 2nd ed.; Cambridge University Press: Cambridge, UK, 1992; p. 994.